

Article

Fluoroquinolone Metalloantibiotics: Fighting *Staphylococcus aureus* Biofilms

Mariana Ferreira ^{1,*}[†], Bruno Ribeiro ^{1,†}, Catarina Leal Seabra ², Ana Rita Ferreira ¹ and Paula Gameiro ¹

¹ LAQV/REQUIMTE (Laboratório Associado para a Química Verde—Rede de Química e Tecnologia), Departamento de Química e Bioquímica, Faculdade de Ciências, Universidade do Porto, Rua do Campo Alegre, s/n, 4169-007 Porto, Portugal; brunoribeirofcupbq@gmail.com (B.R.); ritaferreira@fc.up.pt (A.R.F.); agsantos@fc.up.pt (P.G.)

² LAQV/REQUIMTE, Departamento de Ciências Químicas, Faculdade de Farmácia, Universidade do Porto, 4050-313 Porto, Portugal; cseabra@ff.up.pt

* Correspondence: mariana.ferreira@fc.up.pt

† These authors contributed equally to this work.

Abstract: Antimicrobial resistance (AMR) is one of the biggest public health challenges of this century. The misuse and/or overuse of antibiotics has triggered the rapid development of AMR mechanisms. Fluoroquinolones (FQs) are a broad-spectrum family of antibiotics, widely used in clinical practice. However, several AMR mechanisms against this family have been described. Our strategy to bypass this problem is their complexation with copper and 1,10-phenanthroline (phen). These stable complexes, known as CuFQphen metalloantibiotics, previously proved to be especially effective against methicillin-resistant *Staphylococcus aureus* (MRSA). This work aimed to characterize the interaction of CuFQphen metalloantibiotics with *S. aureus* membranes and to explore their antibiofilm activity with a combination of biophysical and microbiological approaches. Partition constants were assessed for metalloantibiotics in different mimetic systems of *S. aureus* membranes. The thermotropic profiles of the mimetic systems were studied in the absence and presence of the compounds. The antibiofilm activity of the metalloantibiotics was evaluated. The effects of the compounds on the membrane fluidity of MRSA clinical isolates were also investigated. Metalloantibiotics revealed a strong interaction with the lipidic component of the bacterial membranes, preferring cardiolipin-enriched domains. These complexes exhibited antibiofilm activity, and their presence proved to reduce the membrane fluidity of MRSA clinical isolates.

Keywords: fluoroquinolones; metalloantibiotics; antimicrobial resistance; methicillin-resistant *Staphylococcus aureus*



Citation: Ferreira, M.; Ribeiro, B.; Seabra, C.L.; Ferreira, A.R.; Gameiro, P. Fluoroquinolone Metalloantibiotics: Fighting *Staphylococcus aureus* Biofilms. *Micro* **2022**, *2*, 410–425. <https://doi.org/10.3390/micro2030027>

Academic Editor:
Laura Chronopoulou

Received: 10 May 2022

Accepted: 6 July 2022

Published: 8 July 2022

Publisher's Note: MDPI stays neutral with regard to jurisdictional claims in published maps and institutional affiliations.



Copyright: © 2022 by the authors. Licensee MDPI, Basel, Switzerland. This article is an open access article distributed under the terms and conditions of the Creative Commons Attribution (CC BY) license (<https://creativecommons.org/licenses/by/4.0/>).

1. Introduction

One of the major health concerns arising in the 21st century is the rapid development of antimicrobial resistance (AMR) mechanisms in bacteria [1]. AMR occurs when microbes such as bacteria mutate over time and become less and less responsive to treatments used to combat their non-resistant counterparts [1]. Common infections are becoming harder to treat as bacteria become increasingly resistant, and, without urgent global intervention, there is a possibility of a future generation in which regular infections, major surgeries and big sectors of modern medicine could suffer severe setbacks [1]. The development of AMR is accelerated by numerous factors, such as the global misuse of antibiotics in humans and animals but also the poor investment in the development of new antibiotics by pharmaceutical companies [2,3]. Tackling AMR has been a top priority for the World Health Organization (WHO), which considers AMR to be one of the top 10 global public health threats [1].

Fluoroquinolones (FQs) are a broad-spectrum antibiotic family, widely used in clinical practice against Gram-negative and Gram-positive bacteria [4]. The mechanism of action of

FQs consists of the inhibition of bacterial replication by acting on type II topoisomerases, DNA gyrase and topoisomerase IV [5,6]. FQs inhibit DNA supercoiling and relaxation by binding to bacterial enzymes and DNA, stabilizing the enzyme–DNA complex [7] and inhibiting the DNA replication process. However, bacteria exhibit great plasticity to bypass the action of antimicrobial agents through the development of AMR mechanisms. Several AMR mechanisms against FQs have been described, usually involving chromosomal mutations or plasmid-acquired resistance genes (that confer alterations in the target molecules) or a reduction in the intracellular concentration of the drug (by decreasing the influx or improving the efflux) [8–10].

One of the strategies to circumvent AMR against FQs is their complexation with transition metals [11–18]. Among several studies, ternary complexes of FQs, transition metals (especially copper) and 1,10-phenanthroline (phen) have been widely characterized. These complexes, known as CuFQphen metalloantibiotics, (i) are truly stable under physiological concentration, pH and temperature conditions, (ii) exhibit antimicrobial activity against susceptible and multi-drug-resistant (MDR) strains, (iii) share the same mechanism of action of FQs and (iv) adopt an alternative influx route, strongly dependent on interactions with bacterial membranes [15,18–22]. The study of the influx of CuFQphen metalloantibiotics has been widely focused on Gram-negative bacteria due to the complexity of bacterial membranes, which comprise porin channels, which are usually used by free FQs for their translocation [11,17,20–22]. However, CuFQphen metalloantibiotics proved to be especially effective against clinical isolates of methicillin-resistant *Staphylococcus aureus* (MRSA) [19]. To the best of our knowledge, studies on the interaction of CuFQphen metalloantibiotics with Gram-positive bacterial membranes are still lacking. Therefore, this work aimed to characterize the interaction of CuFQphen metalloantibiotics with bacterial membranes of *S. aureus* and further explore their antimicrobial activity against MRSA with a combination of biophysical and microbiological approaches. The work comprised two free FQs, ciprofloxacin (cpx) and moxifloxacin (mxfx), and their respective metalloantibiotics (Cucpxphen and Cumxfxphen). Three lipidic systems—POPG, POPG/CL (58:42) and POPG/CL/DAG (11:5:4)—were chosen to mimic *S. aureus* membranes [23,24]. The partition constants of the compounds were determined in the three lipidic systems by steady-state fluorescence spectroscopy. The thermotropic properties of the mimetic systems were studied in the absence and presence of the compounds by steady-state fluorescence anisotropy. The antibiofilm activity of the metalloantibiotics was also explored against biofilms of susceptible *S. aureus* strains. Membrane fluidity assays were also performed using MRSA clinical isolates to evaluate the possible effect of the metalloantibiotics on membrane fluidity. CuFQphen metalloantibiotics showed a strong interaction with the lipidic component of the bacterial membranes of *S. aureus*, which should be mainly governed by POPG domains. Their location within the membrane seems to favor cardiolipin-enriched domains. CuFQphen metalloantibiotics proved to have antibiofilm activity and to reduce the membrane fluidity of *S. aureus*.

2. Materials and Methods

2.1. Spectroscopic Measurements

Absorption spectra were carried out on a UV–vis–NIR (UV-3600) spectrophotometer (Shimadzu, Kyoto, Japan) equipped with a temperature controller (Shimadzu TCCCONTROLLER). Spectra were recorded at 37.0 ± 0.1 °C in 1 cm quartz cuvettes with a slit width of 5 nm in a wavelength range from 225–450 nm. The FQ and metalloantibiotic concentrations used were chosen according to the Lambert–Beer Law ($abs < 0.1$ at the excitation wavelength) to avoid the inner-filter effect [25,26]. Steady-state fluorescence measurements were performed in a PTI QuantaMaster™ 8075-21 HORIBA spectrofluorometer (HORIBA Scientific, Kyoto, Japan) equipped with a 75 W short arc Xenon lamp (UXL-75XE, Ushio Inc., Tokyo, Japan) and a single emission/excitation monochromator. The fluorescence intensity was recorded in counts per second (cps) in 0.5 cm quartz cuvettes with a 1 nm step size and an integration time of 0.1 s, under stirring at 37.0 ± 0.1 °C. An average of three

fluorescence emission spectra was collected for each sample. Anisotropy measurements and membrane fluidity studies were performed in a Varian Cary Eclipse spectrofluorometer (Agilent Technologies, Santa Clara, CA, USA) equipped with a temperature cell holder (Peltier Multicell Holder, Cary Temperature Probe series II—Agilent Technologies, Santa Clara, CA, USA) coupled to a water circulation thermostat. The temperature of samples in anisotropy experiments was monitored using an in-house-built sensor immersed inside the quartz cuvette.

2.2. Fluoroquinolone and Metalloantibiotic Preparation

All compounds were used as received. Ciprofloxacin (cpx) (>98.0%) was purchased from Sigma-Aldrich (Saint Louis, MO, USA), and moxifloxacin (mxfx) was a gift from Bayer. FQs were stored at room temperature and protected from light. Stock solutions of 1,10-phenanthroline (phen, Sigma-Aldrich), $\text{Cu}(\text{NO}_3)_2 \cdot 3\text{H}_2\text{O}$ (Merck, Darmstadt, Germany), FQs (cpx and mxfx) and respective metalloantibiotics (Cucpxphen and Cumxfxphen) were prepared in 10 mmol dm^{-3} N-(2-hydroxyethyl)piperazine-*N'*-ethanesulfonic acid (Hepes, Sigma-Aldrich) buffer (0.1 mol dm^{-3} NaCl—Sigma-Aldrich; pH 7.4, using double-deionized water), with the exception of the copper salt solution, prepared in double-deionized water. The metalloantibiotic solutions were prepared by mixing the three components (FQ, Cu(II) and phen) in stoichiometric proportions (1:1:1), as previously reported [19,22]. The copper solution used to prepare the metalloantibiotic solutions was previously titrated in alkaline medium with ethylenediaminetetraacetic acid (EDTA, Sigma-Aldrich) using murexide as the indicator. The solutions were filter-sterilized and stored in small aliquots, protected from light, at 4°C .

2.3. Liposome Preparation

All liposomes were prepared using thin-film hydration followed by the extrusion method [27]. Briefly, chloroform (Sigma-Aldrich) solutions containing the appropriate amounts of the used lipids (1-palmitoyl-2-oleoyl-*sn*-glycero-3-phospho-(1'-*rac*-glycerol)—POPG; 1',3'-bis[1,2-dipalmitoyl-*sn*-glycero-3-phospho]-glycerol (16:0 cardiolipin—CL) and 1-2-dioleoyl-*sn*-glycero-3-phospho-(1'-*rac*-glycerol) (18:1 diacylglycerol—DAG), from Avanti Polar Lipids Inc., Alabaster, AL, USA) were dried under a stream of argon. The obtained films were evaporated under vacuum for at least 3 h to ensure the complete removal of the organic solvent. Multilamellar vesicles (MLVs) were obtained by redispersion of the lipidic film in Hepes buffer. The samples were vortexed, and the vesicles were submitted to five cycles of freezing/thawing using liquid nitrogen and a water bath with a temperature above the phase transition temperature of each lipid system. Large unilamellar vesicles (LUVs) were obtained by 10 times extrusion of MLVs through 100 nm polycarbonate filters (Whatman, Maidstone, UK) on a Lipex biomembrane extruder attached to a water bath. The extrusions were performed above the phase transition temperature of each lipidic system. The size and zeta-potential distributions of the vesicles were determined by dynamic light scattering (DLS) on a Zeta Sizer Nano Zs (Malvern Instruments, Malvern, UK) at $37.0 \pm 0.1^\circ\text{C}$ in Hepes buffer. The refractive indices used were 1.330 for Hepes (water) and 1.400 for lipids, and the viscosity of the dispersant used was 0.6913 cP (water). The final mean particle size was $\sim 100 \text{ nm}$ (polydispersity index < 0.1), and the mean zeta potential was $\sim -31 \text{ mV}$. LUV suspensions were stored at 4°C and protected from light prior to use.

The phospholipid concentration in the liposome suspensions was estimated by phosphate analysis through a modified Bartlett method [28,29].

2.4. Partition Constants Determined by Steady-State Fluorescence Spectroscopy

The interaction of FQs and metalloantibiotics with lipid membrane models was studied by steady-state fluorescence spectroscopy, taking advantage of the intrinsic fluorescence of the compounds. The partition constants (K_p) of the compounds were determined in LUVs of POPG, POPG/CL (58:42) and POPG/CL/DAG (11:5:4) [23,24]. The spectra were recorded at $37.0 \pm 0.1^\circ\text{C}$, with an excitation slit width of 5;5;5 (3.84 nm, 3.98 nm and

3.84 nm, respectively) and an emission slit width of 3;4 (1.54 nm and 1.15 nm, respectively) for Cucpxphen; 3;3;3 and 3;4 for cpx and Cumxfphen; and 2;2;2 and 3;4 for mxfx. The spectra were recorded with an excitation wavelength of 290 nm and an emission wavelength range from 300 to 550 nm. Small aliquots of LUVs of each lipidic system studied were successively added to an aqueous solution of cpx, mxfx or their respective metalloantibiotics ($8 \mu\text{mol dm}^{-3}$ for cpx and mxfx; $7 \mu\text{mol dm}^{-3}$ for Cucpxphen; and $6 \mu\text{mol dm}^{-3}$ for Cumxfphen) to achieve lipid concentrations between 0 (A0) and 1 mmol dm^{-3} (A11). After each addition, the samples were left to incubate for 5 min, after which the emission spectra were recorded under constant stirring. All experimental fluorescence data were corrected for the dilution effect [30], and three independent measurements were performed.

- Steady-state fluorescence data analysis

The FQs and metalloantibiotics used in this work exhibit innate fluorescence properties. Therefore, the partition constants of the compounds in liposomes were determined through the analysis of steady-state fluorescence data.

The partition constant (K_p) of any compound between an aqueous solution and vesicle suspensions is defined by IUPAC (the partition constant is defined by IUPAC as the partition ratio; IUPAC does not recommend the use of the former definition. Its use throughout this work reflects the common practice in the biological literature) as:

$$K_p = \frac{(C_L / C_T) / [L]}{(C_W / C_T) / [W]} \quad (1)$$

where C_T , C_L and C_W represent the total molar drug concentration and the molar concentration of the drug in lipid and aqueous media, respectively. $[L]$ and $[W]$ represent lipid and water molar concentrations, respectively.

K_p was determined without phase separation of drug/liposome suspensions [31]. The following equation was fitted to the experimental data [31,32]:

$$\Delta I = \frac{\Delta I_{max} K_p [L]}{[W] + K_p [L]} \quad (2)$$

where ΔI is the difference between the fluorophore intensity in the presence and absence of the quencher, and $\Delta I_{max} = I_{\infty} - I_0$, where I_{∞} is the limiting value of the fluorescence intensity, I .

The measurable spectral changes due to drug/lipid interaction can be used to obtain the partition constant, as the background signals due to liposome light scattering do not interfere under the experimental conditions used.

Experimental data were analyzed using ORIGIN Pro 9.0 software (OriginLab Corporation, Northampton, MA, USA).

2.5. Thermotropic Properties Determined by Steady-State Fluorescence Anisotropy

For anisotropy experiments, a solution of a fluorescent probe (DPH) was prepared in chloroform. The incorporation of the DPH probe in liposomes was performed by incubation of the probe solution with preformed liposomes in a water bath for 45 min at $65.0 \pm 0.1 \text{ } ^\circ\text{C}$. The anisotropy measurements were performed with a final concentration of LUVs of 2.0 mmol dm^{-3} and a final lipid:probe ratio of 300:1 (mol/mol) [33].

The thermotropic behavior of liposomes labeled with DPH was characterized by steady-state fluorescence anisotropy in the absence and presence of compounds (FQs and metalloantibiotics). The concentrations of the FQs and metalloantibiotics used in the anisotropy experiments were the same as those previously used to determine K_p . The anisotropy measurements were performed with excitation and emission wavelengths of 360/427 nm and with a slit width of 10 nm for excitation and emission. The anisotropy values were recorded at $3 \text{ } ^\circ\text{C}$ intervals in the temperature range from $3 \text{ } ^\circ\text{C}$ to $75 \text{ } ^\circ\text{C}$, after

5 min of stabilization of the temperature, for the binary and ternary lipidic systems. At least three independent anisotropy profiles were obtained for each studied system.

POPG has a transition temperature of $-2\text{ }^{\circ}\text{C}$ [34]. Therefore, the effect of the presence of FQs and metalloantibiotics on the POPG LUVs was evaluated by anisotropy measurements performed at $37.0 \pm 0.1\text{ }^{\circ}\text{C}$.

- Steady-state fluorescence anisotropy data analysis

Steady-state fluorescence anisotropy (r_s) is an established parameter that can be interpreted in terms of lipid mobility and membrane fluidity [35]. Since any lipid undergoes a sudden fluidity change at temperatures above their transition temperature (T_m), the use of steady-state fluorescence anisotropy is a well-established method for determining lipid T_m temperatures [33].

Anisotropy values (r_s) are defined by the equation [35]:

$$r_s = \frac{I_{VV} - I_{VHG}}{I_{VV} + 2 I_{VHG}} \quad (3)$$

where I_{VV} and I_{VH} represent the emission intensities when the polarizers are oriented vertical-vertical (parallel) and vertical-horizontal (perpendicular) to the excitation beam. G is a correction factor and is given by the ratio of vertical to horizontal components when the excitation light is polarized in the horizontal direction, $G = I_{HV}/I_{HH}$. The anisotropy values shown are the mean of five independent measurements ($n = 5$).

Raw r_s data were analyzed using ORIGIN Pro 9.0 software as a function of temperature, and the following equation was fitted to the experimental data:

$$r_s = r_{s2} + \frac{r_{s1} - r_{s2}}{1 + 10^{B'(\frac{T}{T_m-1})}} \quad (4)$$

where T is the absolute temperature, T_m is the midpoint phase transition, and r_{s1} and r_{s2} are the upper and lower values of r_s . B' is the slope factor and correlated with the extent of cooperativity (B), given by $B = [1 - 1/(1 + B')]$; the introduction of B yields a convenient scale of cooperativity ranging from 0 to 1 [36].

2.6. Antibiofilm Activity

2.6.1. Bacterial Strains and Growth Conditions

In this study, two *Staphylococcus aureus* strains were used: ATCC 25923 (purchased from American Type Culture Collection, ATCC, Washington DC, USA) and one methicillin-resistant *S. aureus* (MRSA) clinical isolate, Sa3 (kindly provided by Centro Hospitalar Universitário do Porto, Porto, Portugal). Bacteria were grown on Mueller–Hinton agar (MHA, Liofilchem s.r.l, Roseto degli Abruzzi, Teramo, Italy) from stock cultures. MHA plates were incubated at $37.0 \pm 0.1\text{ }^{\circ}\text{C}$ prior to obtaining fresh cultures for each in vitro bioassay.

2.6.2. Biofilm Treatment Assay

The efficacy of metalloantibiotics on established biofilms of *S. aureus* ATCC 25923 was assessed, given the promising antibacterial activity of metalloantibiotics previously described against *S. aureus* [19].

Fresh bacterial cultures were obtained by overnight (16–20 h) incubation of MHA plates at $37.0 \pm 0.1\text{ }^{\circ}\text{C}$. Bacterial suspensions of 1×10^6 colony-forming units (CFU)/mL, prepared in Tryptic Soy Broth (TSB, Sigma-Aldrich), were dispensed into a 96-well microtiter plate (200 μL /well) and incubated at $37.0 \pm 0.1\text{ }^{\circ}\text{C}$ for 24 h to allow biofilm formation. After 24 h, the planktonic phase was discarded, and the biofilms were rinsed twice with PBS buffer (10 mmoldm⁻³ Na₂HPO₄ (Sigma-Aldrich); 1.8 mmoldm⁻³ KH₂PO₄ (Sigma-Aldrich); 137 mmoldm⁻³ NaCl; 2.7 mmoldm⁻³ KCl (Sigma-Aldrich); pH 7.4) and further treated with different concentrations of metalloantibiotics (minimum inhibitory concentration—MIC, 2× MIC, 4× MIC, 8× MIC, 16× MIC and 32× MIC) for 24h. Cpx was

also tested as a FQ control compound. The MIC values of each compound against *S. aureus* ATCC 25923 were previously reported by our research group (MIC cpx = 0.36 $\mu\text{mol dm}^{-3}$; MIC Cucpxphen = 0.36 $\mu\text{mol dm}^{-3}$; MIC Cumxfxphen = 0.08 $\mu\text{mol dm}^{-3}$) [19]. Control wells containing TSB, inoculum and compounds were employed.

The metabolic activity of the biofilms was evaluated by the 3-(4,5-dimethylthiazol-2-yl)-2,5-diphenyltetrazolium bromide (MTT, Sigma-Aldrich) assay, and the quantification of the total biomass was assessed by the crystal violet (Liofilchem s.r.l) assay.

All conditions were studied in six replicates, and three independent experiments were performed. All assays were performed in a Class II Biohazard Safety Cabinet from ESCO (Esco Lifesciences, Singapore).

- MTT Assay

Biofilm viability was assessed by the MTT assay [37]. Briefly, biofilms were rinsed with PBS buffer and incubated (100 μL /well) with MTT solution (0.5 mg/mL, prepared in TSB) for 30 min at 37.0 ± 0.1 °C in the dark. Dimethyl sulfoxide (DMSO, Sigma-Aldrich) was used to extract the formazan dye product (100 μL /well) after MTT removal. The absorbance was measured at 570 nm in a Multiskan GO UV/Vis microplate spectrophotometer (Thermo Fisher Scientific, Waltham, MA, USA). The negative control was prepared using pure DMSO, and the positive control was assessed using untreated biofilm. The results were expressed in terms of the percentage of biofilm viability compared to untreated biofilm (positive control).

- Crystal Violet Assay

The quantification of the total biomass of biofilms was assessed by the crystal violet assay [37]. Briefly, biofilms were rinsed with PBS buffer and incubated with methanol (Sigma-Aldrich) (200 μL /well) for 15 min to fix cells. Methanol was then removed, and the 96-well microtiter plates were left to dry for 15 min, after which the crystal violet solution (0.5% *v/v* in water) was added (200 μL /well) and incubated for 5 min at room temperature. The crystal violet solution was then removed, and biofilms were rinsed with deionized water 5 times, air-dried and eluted with acetic acid (33% *v/v* in water, 200 μL /well) to dissolve the crystals. Absorbance was measured at 595 nm in a plate reader. The results were expressed as perceptual changes compared to the control.

The statistical analysis was performed after normalization of the data, and differences between mean values of groups were assessed by one-way ANOVA (Tukey multiple comparisons test) using GraphPad Prism version 8.00 for Windows (GraphPad Software, San Diego, CA, USA). A *p*-value < 0.05 was considered statistically significant.

2.7. Membrane Fluidity Studies

Membrane fluidity studies were carried out as previously reported by Bessa et al. [38]. Briefly, bacterial cells of MRSA clinical isolates (Sa3) were grown in Nutrient Broth (NB—Liofilchem s.r.l.). For each experiment, 50 mL of NB was inoculated with exponentially growing cells to obtain a cell suspension with an optical density of 0.4 at 600 nm (OD_{600}). Strains were also used to inoculate NB containing different concentrations of antibiotics/compounds, specifically $1/2 \times \text{MIC}$, MIC and $2 \times \text{MIC}$. The MIC values of each compound against the Sa3 MRSA clinical isolate were previously reported by our research group (MIC cpx = 386 $\mu\text{mol dm}^{-3}$; MIC Cucpxphen = 90 $\mu\text{mol dm}^{-3}$; MIC mxfx = 292 $\mu\text{mol dm}^{-3}$; MIC Cumxfxphen = 10 $\mu\text{mol dm}^{-3}$) [27]. A blank (bacterial suspension), a control (bacterial suspension with fluorescent probe—Laurdan, Sigma-Aldrich) and samples (bacterial suspension, probe and antibiotic/compound) were prepared (1.5 mL in NB). Samples were centrifuged using an Eppendorf® Minispin® personal microcentrifuge (Eppendorf, Hamburg, Germany) at 10,000 rpm (rotor F-45-12-11—radius 6 cm) for 7–8 min. Pellets were resuspended in 1.5 mL of NB (for blank and control) or NB with compounds (samples). All inocula were incubated at 37.0 ± 0.1 °C for 3 h. The samples were then centrifuged at 10,000 rpm (rotor F-45-12-11—radius 6 cm) for 7–8 min and rinsed twice with Tris-HCl buffer (15 mM; pH 7.4). The samples were resuspended in Tris-HCl (blank) or Tris-HCl containing 10 $\mu\text{mol dm}^{-3}$ of Laurdan (stock solution prepared in dimethylformamide)

and incubated in the dark at 37.0 ± 0.1 °C with shaking (500 rpm) in a Multiskan GO UV/Vis microplate spectrophotometer (Thermo Fisher Scientific) for 1 h. A 1 mL aliquot of unlabeled and labeled samples was transferred to a 1 cm quartz cuvette to obtain Laurdan emission spectra.

- Laurdan generalized polarization measurements

Emission spectra of Laurdan-labeled bacteria were traced at an excitation wavelength of 350 nm, with emission wavelengths from 360 to 600 nm. The excitation generalized polarization (GP_{exc}) was calculated using the following equation [39]:

$$GP_{exc} = \frac{I_{440} - I_{490}}{I_{440} + I_{490}} \quad (5)$$

where I_{440} and I_{490} represent fluorescence intensities at 440 and 490 nm, obtained with an excitation wavelength of 350 nm.

3. Results and Discussion

3.1. Determination of Partition Constants

The study of the interaction of any compound with membranes usually involves the determination of its partition, which is commonly assessed by K_p . The K_p value is strongly influenced by the physical–chemical properties of the compound and by the membrane composition [16]. In this work, we used liposomes of different compositions—POPG, POPG/CL (58:42) and POPG/CL/DAG (11:5:4)—to mimic the bacterial membranes of *S. aureus* [23,24]. Liposomes are membrane mimetic models widely used due to their structural similarity to natural membrane bilayers. The liposome/water model is considered one of the best membrane models to accurately determine the K_p value of a compound [40]. The background signals from liposome scattering were negligible under the used experimental conditions, as shown in Figure 1. The K_p values, determined in this work by fitting Equation (2) to the experimental data (Figure 2), are presented in Table 1.

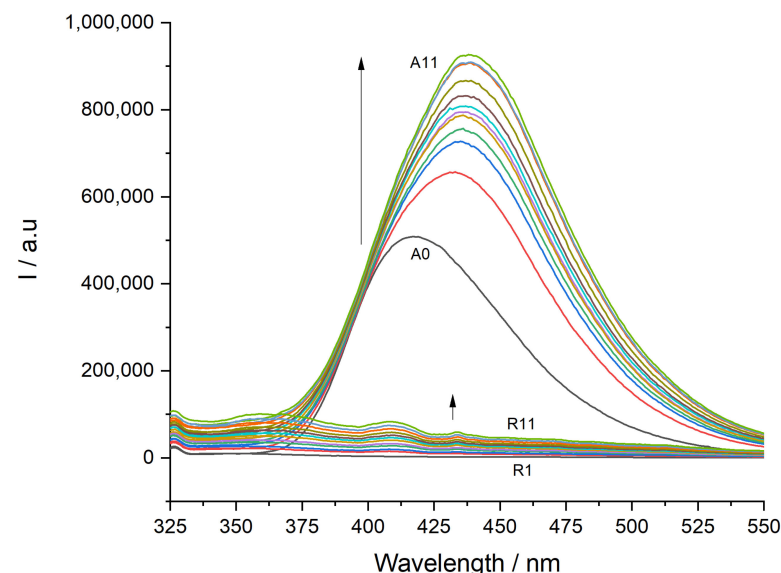


Figure 1. Emission spectra of cpx ($8 \mu\text{mol dm}^{-3}$) in the absence (A0) and presence (A1–A11) of POPG LUVs and respective lipid references (buffer to R11). Liposome concentrations: (R1 and A1) $99 \mu\text{mol dm}^{-3}$; (R2 and A2) $196 \mu\text{mol dm}^{-3}$; (R3 and A3) $291 \mu\text{mol dm}^{-3}$; (R4 and A4) $384 \mu\text{mol dm}^{-3}$; (R5 and A5) $476 \mu\text{mol dm}^{-3}$; (R6 and A6) $566 \mu\text{mol dm}^{-3}$; (R7 and A7) $654 \mu\text{mol dm}^{-3}$; (R8 and A8) $740 \mu\text{mol dm}^{-3}$; (R9 and A9) $826 \mu\text{mol dm}^{-3}$; (R10 and A10) $909 \mu\text{mol dm}^{-3}$; (R11 and A11) $991 \mu\text{mol dm}^{-3}$. Each spectrum is the mean of three replicate measurements.

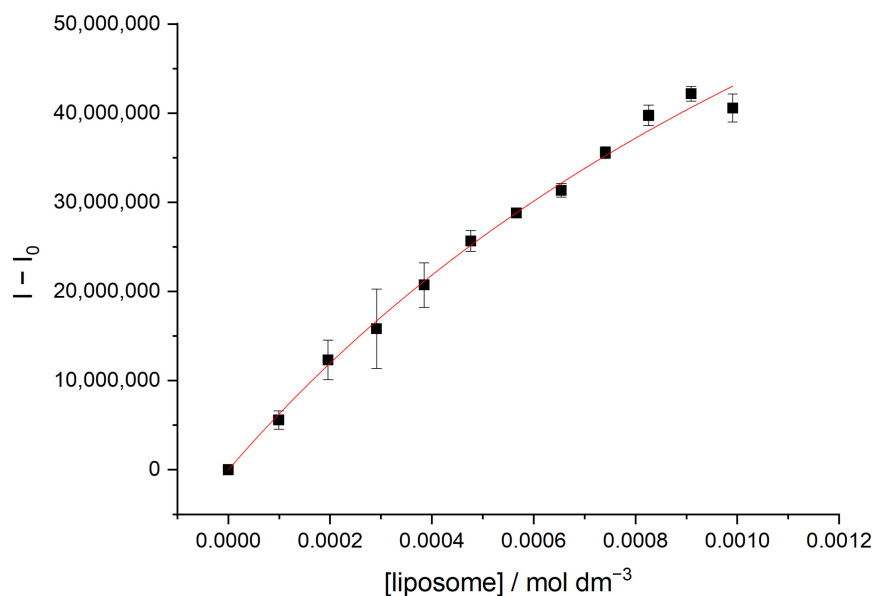


Figure 2. Graphical treatment of the fluorescence data of Cucpxphen ($7 \mu\text{mol dm}^{-3}$) in LUVs of POPG. Equation (2) was fitted to the experimental data. Data points are the means of at least three independent experiments. Error bars are the SD.

Table 1. Values of the partition constants ($K_p \pm SD$) of FQs and metalloantibiotics in different membrane mimetic systems of *Staphylococcus aureus*—POPG, POPG/CL (58:42) and POPG/CL/DAG (11:5:4)—obtained by fluorescence spectroscopy by fitting Equation (2) to the experimental data. The K_p values are the means of three independent experiments.

Membrane Mimetic System	Log K_p			
	cpx	mxfx	Cucpxphen	Cummxphen
POPG	2.72 ± 0.09	3.46 ± 0.07	3.54 ± 0.07	5.20 ± 0.30
POPG:CL (58:42)	2.75 ± 0.08	3.70 ± 0.10	3.73 ± 0.07	N.D.
POPG/CL/DAG (11:5:4)	2.70 ± 0.10	N.D.	N.D.	3.89 ± 0.04

N.D.—not possible to determine with the experimental data obtained.

Emission spectral shifts were observed as a consequence of compound–lipid interactions (Figure 1). For this reason, the integration of the emission fluorescence spectra was performed instead of the use of a single wavelength intensity (Figure 2) [35].

With the exception of Cummxphen, the emission fluorescence spectra revealed an enhancement of the fluorescence intensity and a bathochromic shift to higher wavelengths with the increase in lipid concentration (Figure 1). This trend was previously reported for other FQs and CuFQphen metalloantibiotics and is commonly imputed to the change in polarity surrounding the fluorophore (for a more polar environment) [11,17]. Furthermore, it has been shown that these bathochromic shifts can be attributed to an effective lipid–antibiotic interaction [41]. For Cummxphen, the emission fluorescence spectra evidenced a quenching of the fluorescence, and no shift was observed, pointing out differences in the interaction of this compound (Figure 3).

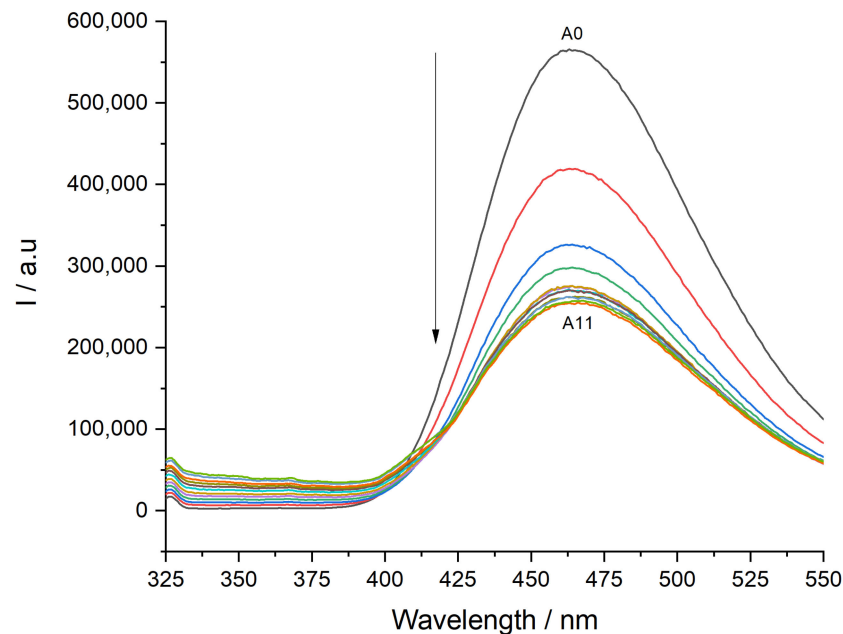


Figure 3. Emission spectra of Cumfxphen ($6 \mu\text{mol dm}^{-3}$) in the absence (A0) and presence (A1–A11) of LUVs of POPG/CL/DAG (11:5:4). Liposome concentrations: (A1) $99 \mu\text{mol dm}^{-3}$; (A2) $196 \mu\text{mol dm}^{-3}$; (A3) $291 \mu\text{mol dm}^{-3}$; (A4) $384 \mu\text{mol dm}^{-3}$; (A5) $476 \mu\text{mol dm}^{-3}$; (A6) $566 \mu\text{mol dm}^{-3}$; (A7) $654 \mu\text{mol dm}^{-3}$; (A8) $740 \mu\text{mol dm}^{-3}$; (A9) $826 \mu\text{mol dm}^{-3}$; (A10) $909 \mu\text{mol dm}^{-3}$; (A11) $991 \mu\text{mol dm}^{-3}$. Each spectrum is the mean of three replicate measurements.

The K_p values (Table 1) revealed a higher partition for metalloantibiotics compared to the respective free FQs. This tendency was previously evidenced for metalloantibiotics in mimetic model systems of Gram-negative bacteria [11,15–17] and is supported by the electrostatic interactions occurring between the positive charge of metalloantibiotics and the negative charge of liposome membranes. Furthermore, these outcomes support an influx route that is strongly dependent on the interaction with the negatively charged bacterial membrane.

The results obtained for cpx and Cucpxphen in POPG agree with data previously reported by Sousa et al. [20]. No significant differences were observed in the partition of each compound in the three studied model systems, which suggests that these compounds may strongly interact with the POPG domains of *S. aureus* membranes.

3.2. Thermotropic Properties of Membranes

Membrane bilayers can exhibit two main thermodynamic phases: a gel phase (more ordered and rigid) and a liquid-disordered or liquid crystalline phase (more fluid and less ordered). The transition between the two phases may still result in an intermedium phase characterized by moderate fluidity and order, the so-called liquid-ordered phase [42,43]. The structural integrity of the membrane is preserved in both phases by electrostatic interactions between water molecules and the polar phospholipid headgroups. The intra- and intermolecular interactions observed in these two phases diverge in the flexibility of the fatty acid chains, being more restricted in the gel phase and less limited in the liquid crystalline phase. The temperature at which the phase change occurs is specific for each lipidic system and is defined as the transition temperature (T_m). As the complexity/heterogeneity of the system rises, there is an expected temperature range between the gel phase and the liquid crystalline phase that corresponds to the coexistence of these two phases (in different proportions), usually exhibiting more than one T.

The T_m of a lipidic system can be determined through the study of anisotropy (r_s) as a function of the temperature due to its sensitivity to changes in the viscosity of the

membranes. In this work, three lipidic compositions were chosen to mimic *S. aureus* membranes: POPG, POPG/CL (58:42) and POPG/CL/DAG (11:5:4) [23,24]. As previously mentioned, POPG has a transition temperature of $-2\text{ }^{\circ}\text{C}$ [34]. Therefore, the anisotropic profile of the DPH probe was assessed in LUVs composed of the binary and ternary mixtures, and the r_s values were determined at $37.0 \pm 0.1\text{ }^{\circ}\text{C}$ for the POPG system. The studies were performed in the absence and presence of FQs and metalloantibiotics to further evaluate the possible interference of the compounds with the fluidity of membranes.

The anisotropic profiles of the DPH (Figure 4) incorporated in LUVs of the binary and ternary mixtures revealed the existence of two transition temperatures (Table 2 and Figure 5), around $10\text{ }^{\circ}\text{C}$ (T_1) and $44\text{ }^{\circ}\text{C}$ (T_2). The values obtained for the two systems are comparable, revealing that the incorporation of DAG does not induce significant changes in the membrane fluidity of the system. Furthermore, the results suggest the existence of domains with distinct compositions: POPG-enriched domains (T_1) and cardiolipin-enriched domains (T_2).

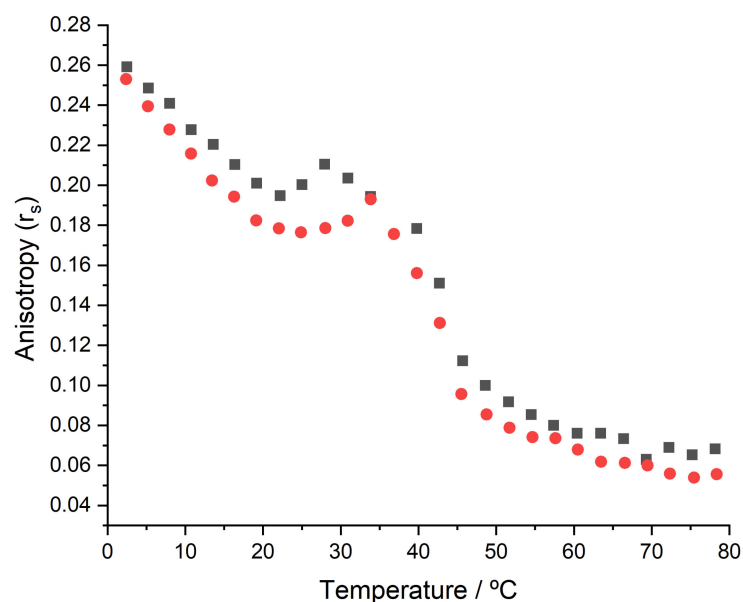


Figure 4. Steady-state fluorescence anisotropy (r_s) of DPH incorporated in LUVs of POPG:CL:DAG (11:5:4), obtained in the absence (black squares) and presence (red circles) of cpx.

Table 2. Transition temperatures ($T \pm \text{SD}$) determined for DPH incorporated in LUVs of POPG:CL (58:42) and POPG:CL:DAG (11:5:4) by steady-state fluorescence anisotropy by fitting Equation (4) to the experimental data. Fluorescence anisotropy values ($r_s \pm \text{SD}$) determined for DPH incorporated in POPG LUVs, obtained by steady-state fluorescence anisotropy. The values were assessed in the absence and presence of compounds and are the means of three independent experiments.

Membrane Mimetic System	Absence of Compound	cpx	mxfx	Cucpxphen	Cumxfxphen
$T_1/^\circ\text{C}$					
POPG:CL (58:42)	10.4 ± 0.3	8.9 ± 0.9	8.0 ± 0.8	9.5 ± 0.1	9.1 ± 0.4
POPG/CL/DAG (11:5:4)	10.7 ± 0.1	9.7 ± 0.2	9.8 ± 0.1	10.3 ± 0.1	10.6 ± 0.1
$T_2/^\circ\text{C}$					
POPG:CL (58:42)	44.8 ± 0.4	46.4 ± 0.1	47.7 ± 0.5	47.4 ± 0.5	45.1 ± 0.4
POPG/CL/DAG (11:5:4)	43.6 ± 0.2	42.5 ± 0.1	42.5 ± 0.2	41.1 ± 0.1	40.9 ± 0.3
r_s Values Determined at $37.0 \pm 0.1\text{ }^{\circ}\text{C}$					
POPG	$5.92 \times 10^{-2} \pm 8.00 \times 10^{-4}$	$6.44 \times 10^{-2} \pm 1.00 \times 10^{-4}$	$6.20 \times 10^{-2} \pm 1.10 \times 10^{-3}$	$7.46 \times 10^{-2} \pm 5.00 \times 10^{-4}$	$8.01 \times 10^{-2} \pm 4.00 \times 10^{-4}$

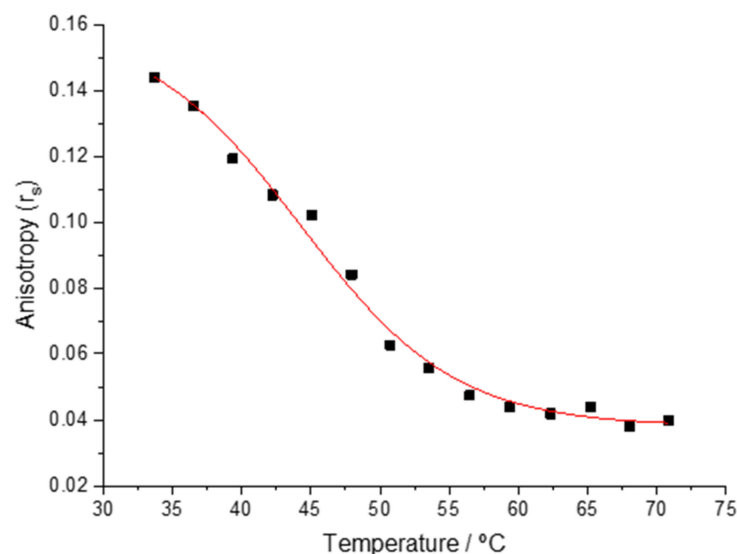


Figure 5. Fitting of Equation (4) to the anisotropic profile of DPH incorporated in LUVs of POPG:CL (58:42), obtained by steady-state fluorescence anisotropy, for the calculation of the transition temperature 2 (T_2).

The anisotropic profiles of the binary and ternary systems revealed some changes in the transition temperatures in the presence of FQs and metalloantibiotics. This interference was more pronounced in the binary system. The presence of FQs resulted in decreases in the value of T_1 of ~ 1 to 2 °C in the binary system and of ~ 1 °C in the ternary system. The presence of the metalloantibiotics had less effect on the value of T_1 , revealing a decrease of ≤ 1 °C in the binary system and no change in the ternary system. The second transition temperature (T_2) of the binary system revealed an increase of ~ 2 to 3 °C in the presence of FQs and of ~ 3 °C in the presence of Cucpxphen. The presence of Cumxfphen did not induce any changes in the value of T_2 of the binary system. In the ternary system, the value of T_2 decreased by ~ 1 °C in the presence of FQs and by ~ 2 to 3 °C in the presence of metalloantibiotics.

Concerning the POPG LUVs, the presence of FQs and metalloantibiotics resulted in an increase in r_s values (determined at 37.0 ± 0.1 °C), being more pronounced in the presence of metalloantibiotics.

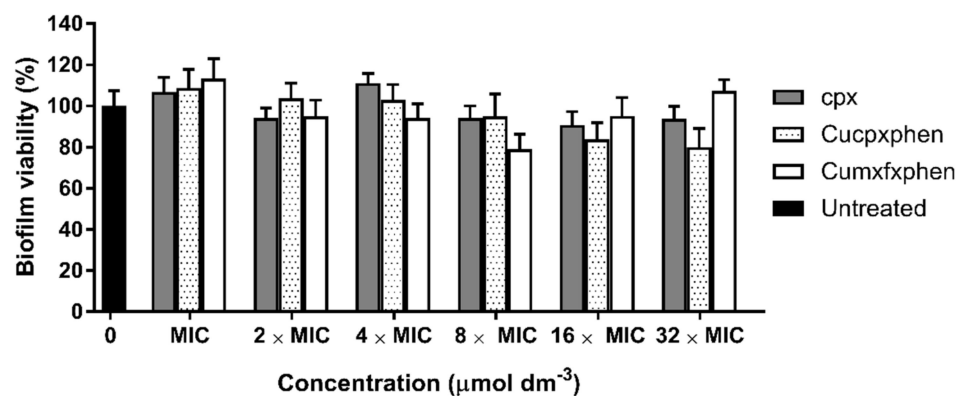
Overall, the presence of metalloantibiotics was revealed to have more impact on the T_2 of the binary and ternary systems, with the exception of Cumxfphen in the binary system. As previously mentioned, T_2 should give information about membrane domains enriched with cardiolipin. Therefore, these findings suggest that metalloantibiotics have a preference for cardiolipin-enriched domains.

3.3. Antibiofilm Activity

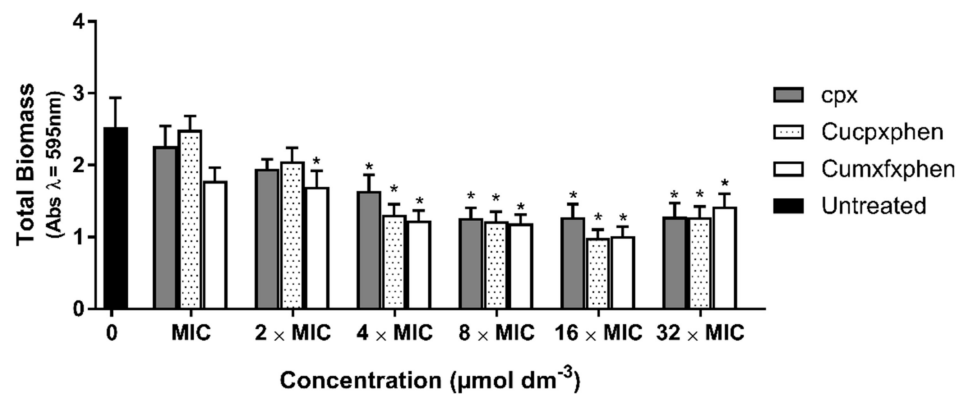
According to the International Organization for Standardization (ISO) 22196:2011 standard, antibacterial activity is the ability of an agent to inhibit the growth of bacteria on a surface, and antibacterial effectiveness is the ability of an antibacterial agent to inhibit the growth of bacteria on a surface treated with the agent, as determined by the value of the antibacterial activity [44]. Antimicrobial activity is usually assessed through the MIC and exhibits the ability of a compound to inhibit the growth of a planktonic bacterial culture [45]. The antimicrobial activity of CuFQphen metalloantibiotics has been widely explored against susceptible and resistant strains of Gram-negative and Gram-positive bacteria. These compounds revealed improved antimicrobial activity against MRSA clinical isolates, revealing MIC values 4- to 28-fold lower than those of free FQs [19]. However, the antibiofilm activity of CuFQphen metalloantibiotics is still lacking. Therefore, preliminary assays were performed to screen the metalloantibiotics for their ability to counteract the

S. aureus biofilm viability and biomass. The antibiofilm experiments should be further explored against biofilms of MRSA clinical isolates.

Biofilms are defined as structured communities of bacterial cells enclosed in self-produced polymeric matrices adhered to surfaces [46]. The antibiofilm activity of a compound measures the ability to fight preformed biofilms or to prevent their formation [45]. The in vitro antibiofilm activity of the metalloantibiotics and cpx was initially assessed by quantification of biofilm viability (Figure 6A) and total biomass (Figure 6B) using the microtiter plate biofilm model for susceptible *S. aureus* ATCC 25923. For all antibiotics tested, the results did not show any significant reduction in bacterial viability at any tested concentration. However, the findings suggest a slight reduction in bacterial viability (around 20%) using metalloantibiotics, namely, at the concentration of $8 \times \text{MIC}$ for Cumxfphen and $16 \times \text{MIC}$ and $32 \times \text{MIC}$ for Cucpxphen, compared to untreated biofilm.



(A)



(B)

Figure 6. Quantification of (A) biofilm viability (MTT assay) and (B) biomass (crystal violet staining) after 24 h treatment with cpx, Cucpxphen and Cumxfphen at different concentrations of MIC to $32 \times \text{MIC}$. MIC cpx = $0.36 \mu\text{mol dm}^{-3}$; MIC Cucpxphen = $0.36 \mu\text{mol dm}^{-3}$; MIC Cumxfphen = $0.08 \mu\text{mol dm}^{-3}$ —MICs previously determined [19]. The values represent the mean \pm SEM. * $p < 0.05$, relatively to $0 \mu\text{mol dm}^{-3}$ (untreated biofilm). Statistical analysis: one-way ANOVA and Tukey multiple comparisons test.

Despite the low antibiofilm activity, the antibiotics showed a significant effect on total biomass at concentrations higher than $4 \times \text{MIC}$, suggesting a destabilization of the extracellular matrix and the bacterial structure and membrane. Previously, Ferreira et al. [19] reported that CuFQphen metalloantibiotics have antibacterial activity against different *S. aureus* strains, including MRSA. However, although these metalloantibiotics showed

slight antibiofilm activity (Figure 6A), their combination with other antibiotics may enhance the antibiofilm efficiency. Previous studies demonstrated that the combination of CuFQphen metalloantibiotics with cpx exhibited a synergistic or additive effect against MRSA [19].

Therefore, some synergistic assays should be performed to evaluate the effect of the combination of these metalloantibiotics with other antibiotics to counteract bacterial biofilms.

3.4. Membrane Fluidity Assays

Laurdan is a polarity-sensitive fluorescent probe that can be used in lipid membranes and in live cells [39]. When incorporated into membranes, this probe provides information about the membrane phase, exhibiting differences in the maximum of the emission spectrum. In liquid-ordered (Lo) phases, Laurdan has a maximum emission at 440 nm (blue shift), while in the liquid-disordered (Ld) phase, the probe shows a maximum at 490 nm (red shift) [47].

The antimicrobial activity of FQs and CuFQphen metalloantibiotics, previously reported, revealed comparable activity of FQs and metalloantibiotics against susceptible strains but evidenced improved antimicrobial activity of metalloantibiotics against MRSA clinical isolates, with MIC values 4- to 28-fold lower than those of free FQs [19]. Therefore, the effects of the FQs and metalloantibiotics (cpx, mxfx, Cucpxphen and Cumxfoxphen) on the membrane fluidity of bacteria were studied in MRSA clinical isolates through the analysis of the fluorescence emission spectra of Laurdan-labeled bacteria and the calculation of excitation generalized polarization (GP_{exc}). Three concentrations of each compound ($1/2 \times MIC$, MIC and $2 \times MIC$) were used. The MIC values of each compound against the Sa3 MRSA clinical isolate were previously reported by our research group (MIC cpx = $386 \mu\text{mol dm}^{-3}$; MIC Cucpxphen = $90 \mu\text{mol dm}^{-3}$; MIC mxfx = $292 \mu\text{mol dm}^{-3}$; MIC Cumxfoxphen = $10 \mu\text{mol dm}^{-3}$) [19].

The results obtained (Table 3 and Figure 7) revealed differences in membrane fluidity in the presence of free FQs and metalloantibiotics.

Table 3. Excitation generalized polarization ($GP_{exc} \pm SD$) values determined for Laurdan-labeled MRSA clinical isolates (Sa3) grown in the absence (control) and presence of different FQ/metalloantibiotic concentrations ($1/2 \times MIC$, MIC and $2 \times MIC$). The values were calculated using Equation (5) and are the means of three independent experiments.

MRSA Sa3	GP_{exc}	[cpx]/ $\mu\text{mol dm}^{-3}$	GP_{exc}	[Cucpxphen]/ $\mu\text{mol dm}^{-3}$
Control	0.245 ± 0.008	0	0.243 ± 0.009	0
$1/2 \times MIC$	0.266 ± 0.005	193	0.409 ± 0.014	45
MIC	0.280 ± 0.006	386	0.426 ± 0.004	90
$2 \times MIC$	0.298 ± 0.005	773	0.418 ± 0.012	180
MRSA Sa3	GP_{exc}	[mxfx]/ $\mu\text{mol dm}^{-3}$	GP_{exc}	[Cumxfoxphen]/ $\mu\text{mol dm}^{-3}$
Control	0.257 ± 0.006	0	0.243 ± 0.009	0
$1/2 \times MIC$	0.285 ± 0.005	146	0.251 ± 0.004	5
MIC	0.295 ± 0.013	292	0.264 ± 0.014	10
$2 \times MIC$	0.289 ± 0.008	585	0.326 ± 0.044	20

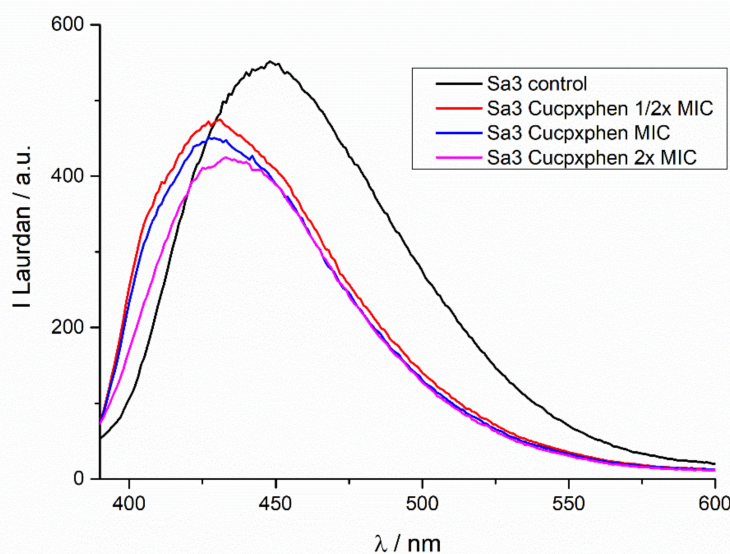


Figure 7. Fluorescence emission spectra of Laurdan-labeled MRSA clinical isolates (Sa3) in the absence (control) and presence of increasing concentrations of Cucpxphen ($1/2 \times \text{MIC}$, MIC and $2 \times \text{MIC}$) metalloantibiotic. MIC of Cucpxphen = $90 \mu\text{mol dm}^{-3}$ —value previously determined [19].

The GP_{exc} values determined in MRSA Sa3 clinical isolates increased in the presence of the studied compounds in comparison to the controls (Table 3). This enhancement was greater as the concentration of the compounds became higher and is indicative of a shift towards the Lo phase. The increases in GP_{exc} values were greater in the presence of metalloantibiotics, revealing that metalloantibiotics induced clear changes in the membrane fluidity of MRSA clinical isolates. Moreover, the Laurdan emission spectra obtained in the absence (control) and presence of the metalloantibiotics revealed an evident shift of the maximum of the spectra to lower wavelengths (Figure 7). This phenomenon was not observed in the presence of free FQs (data not shown).

Previous studies performed by our research group reported that the presence of subinhibitory concentrations of some antibiotics did not alter the membrane fluidity of susceptible and MDR bacteria [38]. In this work, it was possible to conclude that FQs and CuFQphen metalloantibiotics reduce the membrane fluidity of MRSA clinical isolates at concentrations $\geq 1/2 \times \text{MIC}$. The presence of free FQs revealed a slight influence on the membrane fluidity, while metalloantibiotics proved to induce significant changes.

4. Conclusions

The biophysical experiments revealed a higher partition for CuFQphen metalloantibiotics compared to the respective free FQs, mainly governed by the interaction with the POPG domains of *S. aureus* membranes. After influx, these metalloantibiotics may have a preference for cardiolipin-enriched domains, as revealed by anisotropy experiments. On the basis of microbiological studies, CuFQphen metalloantibiotics are suggested to have antibiofilm activity against biofilms of susceptible strains of *S. aureus*. The antibiofilm activity of CuFQphen metalloantibiotics should be further explored against biofilms of MRSA clinical isolates and through synergistic assays. The membrane fluidity assays showed a significant reduction in the membrane fluidity of MRSA clinical isolates in the presence of metalloantibiotics.

Author Contributions: Conceptualization, M.F.; methodology, M.F., A.R.F. and C.L.S.; formal analysis, B.R., M.F., C.L.S. and A.R.F.; investigation, B.R., M.F. and A.R.F.; resources, P.G.; data curation, B.R., M.F. and A.R.F.; writing—original draft preparation, B.R., M.F. and C.L.S.; writing—review and editing, M.F., A.R.F., C.L.S., and P.G.; supervision, M.F., C.L.S. and P.G.; project administration, M.F. and P.G.; funding acquisition, P.G. All authors have read and agreed to the published version of the manuscript.

Funding: This work was financed by National Funds through FCT/MCTES—Portuguese Foundation for Science and Technology within the scope of the project UIDB/50006/2020 and UIDP/50006/2020.

Acknowledgments: The clinical isolates used in this work were obtained from Centro Hospitalar Universitário do Porto, Porto, Portugal, with authorization and approval by Maria Helena Ramos. M.F. thanks FCT and REQUIMTE-LAQV for a post-doc fellowship (REQUIMTE 2019-34). A.R.F. thanks The Medical Biochemistry and Biophysics Doctoral Program (M2B-PhD) and FCT, Portugal, for a PhD fellowship (PD/BD137128/2018).

Conflicts of Interest: The authors declare no conflict of interest.

References

1. World Health Organization. Antibiotic Resistance. Available online: <https://www.who.int/news-room/fact-sheets/detail/antibiotic-resistance> (accessed on 4 May 2022).
2. Spellberg, B.; Gilbert, D.N. The future of antibiotics and resistance: A tribute to a career of leadership by John Bartlett. *Clin. Infect. Dis.* **2014**, *59* (Suppl. S2), S71–S75. [[CrossRef](#)] [[PubMed](#)]
3. Shlaes, D.M.; Sahm, D.; Opiela, C.; Spellberg, B. The FDA reboot of antibiotic development. *Antimicrob. Agents Chemother.* **2013**, *57*, 4605–4607. [[CrossRef](#)]
4. Pham, T.D.M.; Ziora, Z.M.; Blaskovich, M.A.T. Quinolone antibiotics. *MedChemComm* **2019**, *10*, 1719–1739. [[CrossRef](#)]
5. Bush, N.G.; Diez-Santos, I.; Abbott, L.R.; Maxwell, A. Quinolones: Mechanism, Lethality and Their Contributions to Antibiotic Resistance. *Molecules* **2020**, *25*, 5662. [[CrossRef](#)]
6. Fàbrega, A.; Madurga, S.; Giralt, E.; Vila, J. Mechanism of action of and resistance to quinolones. *Microb. Biotechnol.* **2009**, *2*, 40–61. [[CrossRef](#)] [[PubMed](#)]
7. Gellert, M.; Mizuuchi, K.; O’Dea, M.H.; Itoh, T.; Tomizawa, J.I. Nalidixic acid resistance: A second genetic character involved in DNA gyrase activity. *Proc. Natl. Acad. Sci. USA* **1977**, *74*, 4772–4776. [[CrossRef](#)] [[PubMed](#)]
8. Hopkins, K.L.; Davies, R.H.; Threlfall, E.J. Mechanisms of quinolone resistance in *Escherichia coli* and *Salmonella*: Recent developments. *Int. J. Antimicrob. Agents* **2005**, *25*, 358–373. [[CrossRef](#)]
9. Ruiz, J. Transferable Mechanisms of Quinolone Resistance from 1998 Onward. *Clin. Microbiol. Rev.* **2019**, *32*, e00007–e00019. [[CrossRef](#)]
10. Hooper, D.C.; Jacoby, G.A. Mechanisms of drug resistance: Quinolone resistance. *Ann. N. Y. Acad. Sci.* **2015**, *1354*, 12–31. [[CrossRef](#)]
11. Lopes, S.C.; Ribeiro, C.; Gameiro, P. A new approach to counteract bacteria resistance: A comparative study between moxifloxacin and a new moxifloxacin derivative in different model systems of bacterial membrane. *Chem. Biol. Drug Des.* **2013**, *81*, 265–274. [[CrossRef](#)]
12. López-Gresa, M.P.; Ortiz, R.; Perelló, L.; Latorre, J.; Liu-González, M.; García-Granda, S.; Pérez-Priede, M.; Cantón, E. Interactions of metal ions with two quinolone antimicrobial agents (cinoxacin and ciprofloxacin). Spectroscopic and X-ray structural characterization. *Antibacterial studies. J. Inorg. Biochem.* **2002**, *92*, 65–74. [[CrossRef](#)]
13. Wu, G.; Wang, G.; Fu, X.; Zhu, L. Synthesis, Crystal Structure, Stacking Effect and Antibacterial Studies of a Novel Quaternary Copper (II) Complex with Quinolone. *Molecules* **2003**, *8*, 287–296. [[CrossRef](#)]
14. Macías, B.; Villa, M.V.; Rubio, I.; Castiñeiras, A.; Borrás, J. Complexes of Ni(II) and Cu(II) with ofloxacin. Crystal structure of a new Cu(II) ofloxacin complex. *J. Inorg. Biochem.* **2001**, *84*, 163–170. [[CrossRef](#)]
15. Ferreira, M.; Gameiro, P. Fluoroquinolone-Transition Metal Complexes: A Strategy to Overcome Bacterial Resistance. *Microorganisms* **2021**, *9*, 1506. [[CrossRef](#)] [[PubMed](#)]
16. Ferreira, M.; Gameiro, P. Ciprofloxacin metalloantibiotic: An effective antibiotic with an influx route strongly dependent on lipid interaction? *J. Membr. Biol.* **2015**, *248*, 125–136. [[CrossRef](#)]
17. Ribeiro, C.; Lopes, S.C.; Gameiro, P. New Insights into the Translocation Route of Enrofloxacin and Its Metalloantibiotics. *J. Membr. Biol.* **2011**, *241*, 117–125. [[CrossRef](#)]
18. Feio, M.J.; Sousa, I.; Ferreira, M.; Cunha-Silva, L.; Saraiva, R.G.; Queirós, C.; Alexandre, J.G.; Claro, V.; Mendes, A.; Ortiz, R.; et al. Fluoroquinolone–metal complexes: A route to counteract bacterial resistance? *J. Inorg. Biochem.* **2014**, *138*, 129–143. [[CrossRef](#)]
19. Ferreira, M.; Bessa, L.J.; Sousa, C.F.; Eaton, P.; Bongiorno, D.; Stefani, S.; Campanile, F.; Gameiro, P. Fluoroquinolone Metalloantibiotics: A Promising Approach against Methicillin-Resistant *Staphylococcus aureus*. *Int. J. Environ. Res. Public Health* **2020**, *17*, 3127. [[CrossRef](#)]
20. Sousa, C.F.; Coimbra, J.T.S.; Ferreira, M.; Pereira-Leite, C.; Reis, S.; Ramos, M.J.; Fernandes, P.A.; Gameiro, P. Passive Diffusion of Ciprofloxacin and its Metalloantibiotic: A Computational and Experimental study. *J. Mol. Biol.* **2021**, *433*, 166911. [[CrossRef](#)]
21. Sousa, C.F.; Coimbra, J.T.S.; Gomes, I.; Franco, R.; Fernandes, P.A.; Gameiro, P. The binding of free and copper-complexed fluoroquinolones to OmpF porins: An experimental and molecular docking study. *RSC Adv.* **2017**, *7*, 10009–10019. [[CrossRef](#)]
22. Ferreira, M.; Sousa, C.F.; Gameiro, P. Fluoroquinolone Metalloantibiotics to Bypass Antimicrobial Resistance Mechanisms: Decreased Permeation through Porins. *Membranes* **2021**, *11*, 3. [[CrossRef](#)] [[PubMed](#)]

23. Brown, J.S.; Mohamed, Z.J.; Artim, C.M.; Thornlow, D.N.; Hassler, J.F.; Rigoglioso, V.P.; Daniel, S.; Alabi, C.A. Antibacterial isoamphiphathic oligomers highlight the importance of multimeric lipid aggregation for antibacterial potency. *Commun. Biol.* **2018**, *1*, 220. [[CrossRef](#)] [[PubMed](#)]
24. Epanand, R.M.; Epanand, R.F. Lipid domains in bacterial membranes and the action of antimicrobial agents. *Biochim. Biophys. Acta.* **2009**, *1788*, 289–294. [[CrossRef](#)] [[PubMed](#)]
25. Ohno, T. Fluorescence Inner-Filtering Correction for Determining the Humification Index of Dissolved Organic Matter. *Environ. Sci. Technol.* **2002**, *36*, 742–746. [[CrossRef](#)]
26. Cox, L.; Celis, R.; Hermosín, M.C.; Cornejo, J.; Zsolnay, A.; Zeller, K. Effect of Organic Amendments on Herbicide Sorption as Related to the Nature of the Dissolved Organic Matter. *Environ. Sci. Technol.* **2000**, *34*, 4600–4605. [[CrossRef](#)]
27. Zhang, H. Thin-Film Hydration Followed by Extrusion Method for Liposome Preparation. *Methods Mol. Biol.* **2017**, *1522*, 17–22. [[CrossRef](#)] [[PubMed](#)]
28. McClare, C.W. An accurate and convenient organic phosphorus assay. *Anal Biochem.* **1971**, *39*, 527–530. [[CrossRef](#)]
29. Bartlett, G.R. Phosphorus assay in column chromatography. *J. Biol. Chem.* **1959**, *234*, 466–468. [[CrossRef](#)]
30. Coutinho, A.; Prieto, M. Ribonuclease T1 and alcohol dehydrogenase fluorescence quenching by acrylamide: A laboratory experiment for undergraduate students. *J. Chem. Educ.* **1993**, *70*, 425. [[CrossRef](#)]
31. Rodrigues, C.; Gameiro, P.; Reis, S.; Lima, J.L.F.C.; de Castro, B. Interaction of Grepafloxacin with Large Unilamellar Liposomes: Partition and Fluorescence Studies Reveal the Importance of Charge Interactions. *Langmuir* **2002**, *18*, 10231–10236. [[CrossRef](#)]
32. Coutinho, A.; Prieto, M. Self-association of the polyene antibiotic nystatin in dipalmitoylphosphatidylcholine vesicles: A time-resolved fluorescence study. *Biophys. J.* **1995**, *69*, 2541–2557. [[CrossRef](#)]
33. Lopes, S.; Neves, C.S.; Eaton, P.; Gameiro, P. Cardiolipin, a key component to mimic the E. coli bacterial membrane in model systems revealed by dynamic light scattering and steady-state fluorescence anisotropy. *Anal Bioanal. Chem.* **2010**, *398*, 1357–1366. [[CrossRef](#)] [[PubMed](#)]
34. Phase Transition Temperatures for Glycerophospholipids. Available online: <https://avantilipids.com/tech-support/physical-properties/phase-transition-temps> (accessed on 21 April 2022).
35. Lakowicz, J.R. *Principles of Fluorescence Spectroscopy*, 3rd ed.; Springer: Boston, MA, USA, 2006; p. 954. [[CrossRef](#)]
36. Merino-Montero, S.; Montero, M.T.; Hernández-Borrell, J. Effects of lactose permease of Escherichia coli on the anisotropy and electrostatic surface potential of liposomes. *Biophys. Chem.* **2006**, *119*, 101–105. [[CrossRef](#)]
37. Bessa, L.J.; Eaton, P.; Dematei, A.; Plácido, A.; Vale, N.; Gomes, P.; Delerue-Matos, C.; Leite, J.R.S.; Gameiro, P. Synergistic and antibiofilm properties of ocellatin peptides against multidrug-resistant Pseudomonas aeruginosa. *Future Microbiol.* **2018**, *13*, 151–163. [[CrossRef](#)] [[PubMed](#)]
38. Bessa, L.J.; Ferreira, M.; Gameiro, P. Evaluation of membrane fluidity of multidrug-resistant isolates of Escherichia coli and Staphylococcus aureus in presence and absence of antibiotics. *J. Photochem. Photobiol. B.* **2018**, *181*, 150–156. [[CrossRef](#)]
39. Jay, A.G.; Hamilton, J.A. Disorder Amidst Membrane Order: Standardizing Laurdan Generalized Polarization and Membrane Fluidity Terms. *J. Fluoresc.* **2017**, *27*, 243–249. [[CrossRef](#)]
40. Esteves, F.; Moutinho, C.; Matos, C. Correlation between octanol/water and liposome/water distribution coefficients and drug absorption of a set of pharmacologically active compounds. *J. Liposome Res.* **2013**, *23*, 83–93. [[CrossRef](#)]
41. Pávez, P.; Herrera, B.; Toro-Labbé, A.; Encinas, M.V. Structure and medium effects on the photochemical behavior of nonfluorinated quinolone antibiotics. *Photochem. Photobiol.* **2007**, *83*, 511–519. [[CrossRef](#)]
42. Strahl, H.; Errington, J. Bacterial. Membranes: Structure, Domains, and Function. *Annu. Rev. Microbiol.* **2017**, *71*, 519–538. [[CrossRef](#)]
43. Jouhet, J. Importance of the hexagonal lipid phase in biological membrane organization. *Front. Plant Sci.* **2013**, *4*, 494. [[CrossRef](#)]
44. ISO 22196:2011; Measurement of Antibacterial Activity on Plastics and Other Non-Porous Surfaces. International Organization for Standardization: Geneva, Switzerland, 2011.
45. Macia, M.D.; Rojo-Molinero, E.; Oliver, A. Antimicrobial. susceptibility. testing. in. biofilm-growing. bacteria. *Clin. Microbiol. Infect.* **2014**, *20*, 981–990. [[CrossRef](#)] [[PubMed](#)]
46. Miquel, S.; Lagrèfeuille, R.; Souweine, B.; Forestier, C. Anti-biofilm Activity as a Health Issue. *Front. Microbiol.* **2016**, *7*, 592. [[CrossRef](#)] [[PubMed](#)]
47. Bessa, L.J.; Ferreira, M.; Gameiro, P. Data on Laurdan spectroscopic analyses to compare membrane fluidity between susceptible and multidrug-resistant bacteria. *Data Brief* **2018**, *21*, 128–132. [[CrossRef](#)] [[PubMed](#)]